In Proc. 8th European Conference on Computer Vision, Springer LNCS 3024, T. Pajdla and J. Matas (Eds.), vol. 4, pp. 25-36, Prague, Czech Republic, May 2004 **Received The Longuet-Higgins Best Paper Award.**

High Accuracy Optical Flow Estimation Based on a Theory for Warping ⋆

Thomas Brox, Andrés Bruhn, Nils Papenberg, and Joachim Weickert

Mathematical Image Analysis Group
Faculty of Mathematics and Computer Science
Saarland University, Building 27, 66041 Saarbrücken, Germany
{brox,bruhn,papenberg,weickert}@mia.uni-saarland.de
http://www.mia.uni-saarland.de

Abstract. We study an energy functional for computing optical flow that combines three assumptions: a brightness constancy assumption, a gradient constancy assumption, and a discontinuity-preserving spatio-temporal smoothness constraint. In order to allow for large displacements, linearisations in the two data terms are strictly avoided. We present a consistent numerical scheme based on two nested fixed point iterations. By proving that this scheme implements a coarse-to-fine warping strategy, we give a theoretical foundation for warping which has been used on a mainly experimental basis so far. Our evaluation demonstrates that the novel method gives significantly smaller angular errors than previous techniques for optical flow estimation. We show that it is fairly insensitive to parameter variations, and we demonstrate its excellent robustness under noise.

1 Introduction

Optical flow estimation is still one of the key problems in computer vision. Estimating the displacement field between two images, it is applied as soon as correspondences between pixels are needed. Problems of this type are not only restricted to motion estimation, they are also present in a similar fashion in 3D reconstruction or image registration. In the last two decades the quality of optical flow estimation methods has increased dramatically. Starting from the original approaches of Horn and Schunck [11] as well as Lucas and Kanade [15], research developed many new concepts for dealing with shortcomings of previous models. In order to handle discontinuities in the flow field, the quadratic regulariser in the Horn and Schunck model was replaced by smoothness constraints that permit piecewise smooth results [1, 9, 19, 21, 25]. Some of these ideas are close in spirit to methods for joint motion estimation and motion segmentation [10, 17], and to optical flow methods motivated from robust statistics where outliers are penalised less severely [6, 7]. Coarse-to-fine strategies [3, 7, 16] as well as non-linearised models [19, 2] have been used to tackle large displacements. Finally, spatio-temporal approaches have ameliorated the results simply by using the information of an additional dimension [18, 6, 26, 10].

However, not only new ideas have improved the quality of optical flow estimation techniques. Also efforts to obtain a better understanding of what the methods do in detail, and which effects are caused by changing their parameters, gave an insight into how

⋆ We gratefully acknowledge partial funding by the *Deutsche Forschungsgemeinschaft (DFG)*.

several models could work together. Furthermore, variational formulations of models gave access to the long experience of numerical mathematics in solving partly difficult optimisation problems. Finding the optimal solution to a certain model is often not trivial, and often the full potential of a model is not used because concessions to implementation aspects have to be made.

In this paper we propose a novel variational approach that integrates several of the before mentioned concepts and which can be minimised with a solid numerical method. It is further shown that a coarse-to-fine strategy using the so-called warping technique [7, 16], implements the non-linearised optical flow constraint used in [19, 2] and in image registration. This has two important effects: Firstly, it becomes possible to integrate the warping technique, which was so far only algorithmically motivated, into a variational framework. Secondly, it shows a theoretically sound way of how image correspondence problems can be solved with an efficient multi-resolution technique. It should be noted that – apart from a very nice paper by Lefébure and Cohen [14] – not many theoretical results on warping are available so far.

Finally, the grey value constancy assumption, which is the basic assumption in optical flow estimation, is extended by a gradient constancy assumption. This makes the method robust against grey value changes. While gradient constancy assumptions have also been proposed in [23, 22] in order to deal with the aperture problem in the scope of a local approach, their use within variational methods is novel.

The experimental evaluation shows that our method yields excellent results. Compared to those in the literature, their accuracy is always significantly higher, sometimes even twice as high as the best value known so far. Moreover, the method proved also to be robust under a considerable amount of noise and computation times of only a few seconds per frame on contemporary hardware are possible.

Paper organisation. In the next section, our variational model is introduced, first by discussing all model assumptions, and then in form of an energy based formulation. Section 3 derives a minimisation scheme for this energy. The theoretical foundation of warping methods as a numerical approximation step is given in Section 4. An experimental evaluation is presented in Section 5, followed by a brief summary in Section 6.

2 The Variational Model

Before deriving a variational formulation for our optical flow method, we give an intuitive idea of which constraints in our view should be included in such a model.

– **Grey value constancy assumption.**
Since the beginning of optical flow estimation, it has been assumed that the grey value of a pixel is not changed by the displacement.

$$I(x, y, t) = I(x + u, y + v, t + 1) \tag{1}$$

Here $I : \Omega \subset \mathbb{R}^3 \to \mathbb{R}$ denotes a rectangular image sequence, and $\mathbf{w} := (u, v, 1)^\top$ is the searched displacement vector between an image at time t and another image at time $t + 1$. The linearised version of the grey value constancy assumption yields the famous optical flow constraint [11]

$$I_x u + I_y v + I_t = 0 \tag{2}$$

where subscripts denote partial derivatives. However, this linearisation is only valid under the assumption that the image changes linearly along the displacement, which is in general not the case, especially for large displacements. Therefore, our model will use the original, non-linearised grey value constancy assumption (1).

– **Gradient constancy assumption.**
The grey value constancy assumption has one decisive drawback: It is quite susceptible to slight changes in brightness, which often appear in natural scenes. Therefore, it is useful to allow some small variations in the grey value and help to determine the displacement vector by a criterion that is invariant under grey value changes. Such a criterion is the gradient of the image grey value, which can also be assumed not to vary due to the displacement [23]. This gives

$$\nabla I(x, y, t) = \nabla I(x + u, y + v, t + 1). \tag{3}$$

Here $\nabla = (\partial_x, \partial_y)^\top$ denotes the spatial gradient. Again it can be useful to refrain from a linearisation. The constraint (3) is particularly helpful for translatory motion, while constraint (2) can be better suited for more complicated motion patterns.

– **Smoothness assumption.**
So far, the model estimates the displacement of a pixel only locally without taking any interaction between neighbouring pixels into account. Therefore, it runs into problems as soon as the gradient vanishes somewhere, or if only the flow in normal direction to the gradient can be estimated (*aperture problem*). Furthermore, one would expect some outliers in the estimates. Hence, it is useful to introduce as a further assumption the smoothness of the flow field. This smoothness constraint can either be applied solely to the spatial domain, if there are only two frames available, or to the spatio-temporal domain, if the displacements in a sequence of images are wanted. As the optimal displacement field will have discontinuities at the boundaries of objects in the scene, it is sensible to generalise the smoothness assumption by demanding a *piecewise smooth* flow field.

– **Multiscale approach.**
In the case of displacements that are larger than one pixel per frame, the cost functional in a variational formulation must be expected to be multi-modal, i.e. a minimisation algorithm could easily be trapped in a local minimum. In order to find the global minimum, it can be useful to apply multiscale ideas: One starts with solving a coarse, smoothed version of the problem by working on the smoothed image sequence. The new problem may have a unique minimum, hopefully close to the global minimum of the original problem. The coarse solution is used as initialisation for solving a refined version of the problem until step by step the original problem is solved. Instead of smoothing the image sequence, it is more efficient to downsample the images respecting the sampling theorem, so the model ends up in a multiresolution strategy.

With this description, it is straightforward to derive an energy functional that penalises deviations from these model assumptions. Let $\mathbf{x} := (x, y, t)^\top$ and $\mathbf{w} := (u, v, 1)^\top$. Then the global deviations from the grey value constancy assumption and the gradient

constancy assumption are measured by the energy

$$E_{Data}(u,v) = \int_\Omega \left(|I(\mathbf{x}+\mathbf{w}) - I(\mathbf{x})|^2 + \gamma|\nabla I(\mathbf{x}+\mathbf{w}) - \nabla I(\mathbf{x})|^2\right) \mathbf{dx} \quad (4)$$

with γ being a weight between both assumptions. Since with quadratic penalisers, outliers get too much influence on the estimation, an increasing concave function $\Psi(s^2)$ is applied, leading to a robust energy [7, 16]:

$$E_{Data}(u,v) = \int_\Omega \Psi\left(|I(\mathbf{x}+\mathbf{w}) - I(\mathbf{x})|^2 + \gamma|\nabla I(\mathbf{x}+\mathbf{w}) - \nabla I(\mathbf{x})|^2\right) \mathbf{dx} \quad (5)$$

The function Ψ can also be applied separately to each of these two terms. We use the function $\Psi(s^2) = \sqrt{s^2+\epsilon^2}$ which results in (modified) L^1 minimisation. Due to the small positive constant ϵ, $\Psi(s)$ is still convex which offers advantages in the minimisation process. Moreover, this choice of Ψ does not introduce any additional parameters, since ϵ is only for numerical reasons and can be set to a fixed value, which we choose to be 0.001.

Finally, a smoothness term has to describe the model assumption of a piecewise smooth flow field. This is achieved by penalising the total variation of the flow field [20, 8], which can be expressed as

$$E_{Smooth}(u,v) = \int_\Omega \Psi\left(|\nabla_3 u|^2 + |\nabla_3 v|^2\right) \mathbf{dx}. \quad (6)$$

with the same function for Ψ as above. The spatio-temporal gradient $\nabla_3 := (\partial_x, \partial_y, \partial_t)^\top$ indicates that a spatio-temporal smoothness assumption is involved. For applications with only two images available it is replaced by the spatial gradient.

The total energy is the weighted sum between the data term and the smoothness term

$$E(u,v) = E_{Data} + \alpha E_{Smooth} \quad (7)$$

with some regularisation parameter $\alpha > 0$. Now the goal is to find the functions u and v that minimise this energy.

3 Minimisation

3.1 Euler–Lagrange Equations

Since $E(u,v)$ is highly nonlinear, the minimisation is not trivial. For better readability we define the following abbreviations, where the use of z instead of t emphasises that the expression is *not* a temporal derivative but a difference that is sought to be minimised.

$$\begin{aligned}
I_x &:= \partial_x I(\mathbf{x}+\mathbf{w}),\\
I_y &:= \partial_y I(\mathbf{x}+\mathbf{w}),\\
I_z &:= I(\mathbf{x}+\mathbf{w}) - I(\mathbf{x}),\\
I_{xx} &:= \partial_{xx} I(\mathbf{x}+\mathbf{w}),\\
I_{xy} &:= \partial_{xy} I(\mathbf{x}+\mathbf{w}),\\
I_{yy} &:= \partial_{yy} I(\mathbf{x}+\mathbf{w}),\\
I_{xz} &:= \partial_x I(\mathbf{x}+\mathbf{w}) - \partial_x I(\mathbf{x}),\\
I_{yz} &:= \partial_y I(\mathbf{x}+\mathbf{w}) - \partial_y I(\mathbf{x}).
\end{aligned} \quad (8)$$

According to the calculus of variations, a minimiser of (7) must fulfill the Euler-Lagrange equations

$$\begin{aligned}
&\Psi'(I_z^2+\gamma(I_{xz}^2+I_{yz}^2))\cdot(I_xI_z+\gamma(I_{xx}I_{xz}+I_{xy}I_{yz}))\\
&\qquad\qquad -\alpha \text{ div } \left(\Psi'(|\nabla_3 u|^2+|\nabla_3 v|^2)\nabla_3 u\right)=0,\\
&\Psi'(I_z^2+\gamma(I_{xz}^2+I_{yz}^2))\cdot(I_yI_z+\gamma(I_{yy}I_{yz}+I_{xy}I_{xz}))\\
&\qquad\qquad -\alpha \text{ div } \left(\Psi'(|\nabla_3 u|^2+|\nabla_3 v|^2)\nabla_3 v\right)=0
\end{aligned}$$

with reflecting boundary conditions.

3.2 Numerical Approximation

The preceding Euler-Lagrange equations are nonlinear in their argument $\mathbf{w}=(u,v,1)^\top$. A first step towards a linear system of equations, which can be solved with common numerical methods, is the use of fixed point iterations on $\mathbf{w}$. In order to implement a multiscale approach, necessary to better approximate the global optimum of the energy, these fixed point iterations are combined with a downsampling strategy. Instead of the standard downsampling factor of 0.5 on each level, it is proposed here to use an *arbitrary* factor $\eta\in(0,1)$, what allows smoother transitions from one scale to the next[1]. Moreover, the full pyramid of images is used, starting with the smallest possible image at the coarsest grid. Let $\mathbf{w}^k=(u^k,v^k,1)^\top$, $k=0,1,\ldots$, with the initialisation $\mathbf{w}^0=(0,0,1)^\top$ at the coarsest grid. Further, let I_*^k be the abbreviations defined in (8) but with the iteration variable $\mathbf{w}^k$ instead of $\mathbf{w}$. Then $\mathbf{w}^{k+1}$ will be the solution of

$$\begin{aligned}
&\Psi'((I_z^{k+1})^2+\gamma((I_{xz}^{k+1})^2+(I_{yz}^{k+1})^2))\cdot(I_x^kI_z^{k+1}+\gamma(I_{xx}^kI_{xz}^{k+1}+I_{xy}^kI_{yz}^{k+1}))\\
&\qquad\qquad -\alpha \text{ div } \left(\Psi'(|\nabla_3 u^{k+1}|^2+|\nabla_3 v^{k+1}|^2)\nabla_3 u^{k+1}\right)=0\\
&\Psi'((I_z^{k+1})^2+\gamma((I_{xz}^{k+1})^2+(I_{yz}^{k+1})^2))\cdot(I_y^kI_z^{k+1}+\gamma(I_{yy}^kI_{yz}^{k+1}+I_{xy}^kI_{xz}^{k+1}))\\
&\qquad\qquad -\alpha \text{ div } \left(\Psi'(|\nabla_3 u^{k+1}|^2+|\nabla_3 v^{k+1}|^2)\nabla_3 v^{k+1}\right)=0.
\end{aligned}\tag{9}$$

As soon as a fixed point in $\mathbf{w}^k$ is reached, we change to the next finer scale and use this solution as initialisation for the fixed point iteration on this scale.
Notice that we have a fully implicit scheme for the smoothness term and a semi-implicit scheme for the data term. Implicit schemes are used to yield higher stability and faster convergence. However, this new system is still nonlinear because of the nonlinear function Ψ' and the symbols I_*^{k+1}. In order to remove the nonlinearity in I_*^{k+1}, first order Taylor expansions are used:

$$\begin{aligned}
I_z^{k+1}&\approx I_z^k+I_x^kdu^k+I_y^kdv^k,\\
I_{xz}^{k+1}&\approx I_{xz}^k+I_{xx}^kdu^k+I_{xy}^kdv^k,\\
I_{yz}^{k+1}&\approx I_{yz}^k+I_{xy}^kdu^k+I_{yy}^kdv^k,
\end{aligned}$$

[1] Since the grid size in both x- and y-direction is reduced by η, the image size in fact shrinks with a factor η^2 at each scale.

where $u^{k+1} = u^k + du^k$ and $v^{k+1} = v^k + dv^k$. So we split the unknowns u^{k+1}, v^{k+1} in the solutions of the previous iteration step u^k, v^k and unknown increments du^k, dv^k. For better readability let

$$\begin{aligned}(\Psi')^k_{Data} \quad &:= \Psi'\Big((I^k_z + I^k_x du^k + I^k_y dv^k)^2 \\ &\qquad + \gamma\big((I^k_{xz} + I^k_{xx} du^k + I^k_{xy} dv^k)^2 + (I^k_{yz} + I^k_{xy} du^k + I^k_{yy} dv^k)^2\big)\Big), \\ (\Psi')^k_{Smooth} &:= \Psi'(|\nabla_3(u^k + du^k)|^2 + |\nabla_3(v^k + dv^k)|^2),\end{aligned} \tag{10}$$

where $(\Psi')^k_{Data}$ can be interpreted as a robustness factor in the data term, and $(\Psi')^k_{Smooth}$ as a diffusivity in the smoothness term. With this the first equation in system (9) can be written as

$$\begin{aligned}0 &= (\Psi')^k_{Data} \cdot \Big(I^k_x \left(I^k_z + I^k_x du^k + I^k_y dv^k\right)\Big) \\ &\quad + \gamma\,(\Psi')^k_{Data} \cdot \Big(I^k_{xx}(I^k_{xz} + I^k_{xx} du^k + I^k_{xy} dv^k) + I^k_{xy}(I^k_{yz} + I^k_{xy} du^k + I^k_{yy} dv^k)\Big) \\ &\quad - \alpha \text{ div } \left((\Psi')^k_{Smooth} \nabla_3(u^k + du^k)\right),\end{aligned} \tag{11}$$

and the second equation can be expressed in a similar way. This is still a nonlinear system of equations for a fixed k, but now in the unknown increments du^k, dv^k. As the only remaining nonlinearity is due to Ψ', and Ψ has been chosen to be a convex function, the remaining optimisation problem is a convex problem, i.e. there exists a unique minimum solution.

In order to remove the remaining nonlinearity in Ψ', a second, inner, fixed point iteration loop is applied. Let $du^{k,0} := 0$, $dv^{k,0} := 0$ be our initialisation and let $du^{k,l}, dv^{k,l}$ denote the iteration variables at some step l. Furthermore, let $(\Psi')^{k,l}_{Data}$ and $(\Psi')^{k,l}_{Smooth}$ denote the robustness factor and the diffusivity defined in (10) at iteration k, l. Then finally the *linear* system of equations in $du^{k,l+1}, dv^{k,l+1}$ reads

$$\begin{aligned}0 &= (\Psi')^{k,l}_{Data} \cdot \Big(I^k_x \left(I^k_z + I^k_x du^{k,l+1} + I^k_y dv^{k,l+1}\right) \\ &\quad + \gamma I^k_{xx}(I^k_{xz} + I^k_{xx} du^{k,l+1} + I^k_{xy} dv^{k,l+1}) + \gamma I^k_{xy}(I^k_{yz} + I^k_{xy} du^{k,l+1} + I^k_{yy} dv^{k,l+1})\Big) \\ &\quad - \alpha \text{ div } \Big((\Psi')^{k,l}_{Smooth} \nabla_3(u^k + du^{k,l+1})\Big)\end{aligned} \tag{12}$$

for the first equation. Using standard discretisations for the derivatives, the resulting sparse linear system of equations can now be solved with common numerical methods, such as Gauss-Seidel or SOR iterations. Expressions of type $I(\mathbf{x} + \mathbf{w^k})$ are computed by means of bilinear interpolation.

4 Relation to Warping Methods

Coarse-to-fine warping techniques are a frequently used tool for improving the performance of optic flow methods [3, 7, 17]. While they are often introduced on a purely experimental basis, we show in this section that they can be theoretically justified as a numerical approximation.

In order to establish this relation, we restrict ourselves to the grey value constancy model by setting $\gamma = 0$. Let us also simplify the model by assuming solely spatial smoothness, as in [17]. Under these conditions, (11) can be written as

$$\begin{aligned}&(\Psi')^k_{Data}\nabla I^k(\nabla I^k)^\top \begin{pmatrix} du^k \\ dv^k \end{pmatrix} - \alpha \begin{pmatrix} \text{div } \left((\Psi')^k_{Smooth}\nabla(u^k + du^k)\right) \\ \text{div } \left((\Psi')^k_{Smooth}\nabla(v^k + dv^k)\right) \end{pmatrix} \\ &= -(\Psi')^k_{Data} I^k_z \nabla I^k \end{aligned} \tag{13}$$

For a fixed k, this system is equivalent to the Euler–Lagrange equations described in [17]. Also there, only the increments du and dv between the first image and the warped second image are estimated. The same increments appear in the outer fixed point iterations of our approach in order to resolve the nonlinearity of the grey value constancy assumption. *This shows that the warping technique implements the minimisation of a non-linearised constancy assumption by means of fixed point iterations on* w.
In earlier approaches, the main motivation for warping has been the coarse-to-fine strategy. Due to solutions u and v computed on coarser grids, only an increment du and dv had to be computed on the fine grid. Thus, the estimates used to have a magnitude of less than one pixel per frame, independent of the magnitude of the total displacement. This ability to deal with larger displacements proved to be a very important aspect in differential optical flow estimation.
A second strategy to deal with large displacements has been the usage of the non-linearised grey value constancy assumption [19, 2]. Here, large displacements are allowed from the beginning. However, the nonlinearity results in a multi-modal functional. In such a setting, the coarse-to-fine strategy is not only wanted, but even necessary to better approximate the global minimum. At the end, both strategies not only lead to similar results. In fact, as we have seen above, they are completely equivalent. As a consequence, the coarse-to-fine warping technique can be formulated as a single minimisation problem, and image registration techniques relying on non-linearised constancy assumptions get access to an efficient multiresolution method for minimising their energy functionals.

5 Evaluation

For evaluation purposes experiments with both synthetic and real-world image data were performed. The presented angular errors were computed according to [5].
Let us start our evaluation with the two variants of a famous sequence: the *Yosemite* sequence with and without cloudy sky. The original version with cloudy sky was created by Lynn Quam and is available at `ftp://ftp.csd.uwo.ca/pub/vision`. It combines both divergent and translational motion. The version without clouds is available at `http://www.cs.brown.edu/people/black/images.html`.
Tab.1 shows a comparison of our results for both sequences to the best results from the literature. As one can see, our variational approach outperforms all other methods. Regarding the sequence with clouds, we achieve results that are more than twice as accurate as all results from the literature. For the sequence without clouds, angular errors below 1 degree are reached for the first time with a method that offers full density. The

Yosemite with clouds		
Technique	AAE	STD
Nagel [5]	10.22°	16.51°
Horn–Schunck, mod. [5]	9.78°	16.19°
Uras *et al.* [5]	8.94°	15.61°
Alvarez *et al.* [2]	5.53°	7.40°
Weickert *et al.* [24]	5.18°	8.68°
Mémin–Pérez [16]	4.69°	6.89°
Our method (2D)	**2.46°**	**7.31°**
Our method (3D)	**1.94°**	**6.02°**

Yosemite without clouds		
Technique	AAE	STD
Ju *et al.* [12]	2.16°	2.00°
Bab-Hadiashar–Suter [4]	2.05°	2.92°
Lai–Vemuri [13]	1.99°	1.41°
Our method (2D)	**1.59°**	**1.39°**
Mémin–Pérez [16]	1.58°	1.21°
Weickert *et al.* [24]	1.46°	1.50°
Farnebäck [10]	1.14°	2.14°
Our method (3D)	**0.98°**	**1.17°**

Table 1. Comparison between the results from the literature with 100 % density and our results for the *Yosemite* sequence with and without cloudy sky. AAE = average angular error. STD = standard deviation. 2D = spatial smoothness assumption. 3D = spatio-temporal smoothness assumption.

Yosemite with clouds		
σ_n	AAE	STD
0	1.94°	6.02°
10	2.50°	5.96°
20	3.12°	6.24°
30	3.77°	6.54°
40	4.37°	7.12°

Yosemite without clouds		
σ_n	AAE	STD
0	0.98°	1.17°
10	1.26°	1.29°
20	1.63°	1.39°
30	2.03°	1.53°
40	2.40°	1.71°

Table 2. Results for the *Yosemite* sequence with and without cloudy sky. Gaussian noise with varying standard deviations σ_n was added, and the average angular errors and their standard deviations were computed. AAE = average angular error. STD = standard deviation.

corresponding flow fields presented in Fig.1 give a qualitative impression of these raw numbers: They match the ground truth very well. Not only the discontinuity between the two types of motion is preserved, also the translational motion of the clouds is estimated accurately. The reason for this behaviour lies in our assumptions, that are clearly stated in the energy functional: While the choice of the smoothness term allows discontinuities, the gradient constancy assumption is able to handle brightness changes – like in the area of the clouds.

Because of the presence of second order image derivatives in the Euler-Lagrange equations, we tested the influence of noise on the performance of our method in the next experiment. We added Gaussian noise of mean zero and different standard deviations to both sequences. The obtained results are presented in Tab.2. They show that our approach even yields excellent flow estimates when severe noise is present: For the cloudy Yosemite sequence, our average angular error for noise with standard deviation 40 is better than all results from the literature for the sequence *without* noise.

In a third experiment we evaluated the robustness of the free parameters in our approach: the weight γ between the grey value and the gradient constancy assumption, and the smoothness parameter α. Often an image sequence is preprocessed by Gaus-

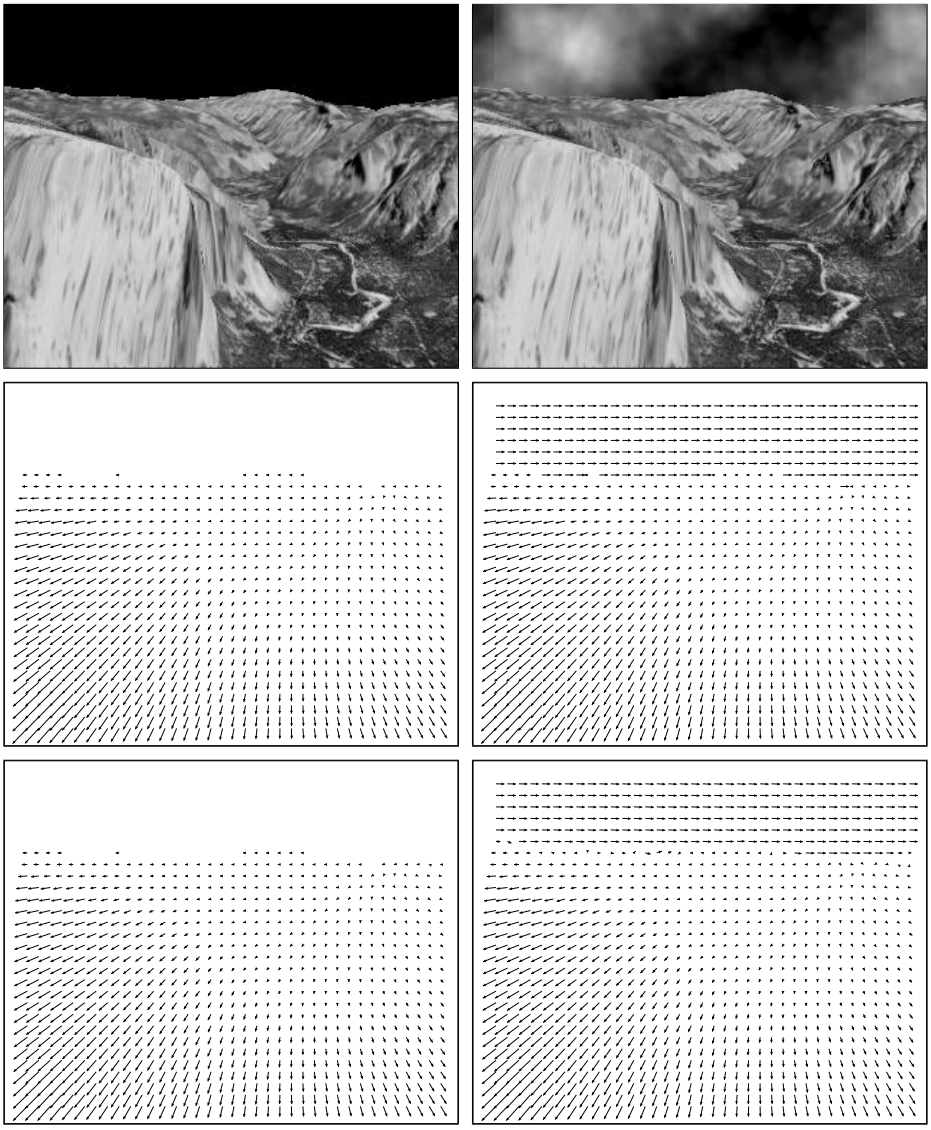

Fig. 1. *(a) Top left:* Frame 8 of the *Yosemite* sequence without clouds. *(b) Top right:* Corresponding frame of the sequence *with* clouds. *(c) Middle left:* Ground truth without clouds. *(d) Middle right:* Ground truth *with* clouds. *(e) Bottom left:* Computed flow field by our 3D method for the sequence without clouds. *(f) Bottom right:* Ditto for the sequence *with* clouds.

sian convolution with standard deviation σ [5]. In this case, σ can be regarded as a third parameter. We computed results with parameter settings that deviated by a factor 2 in both directions from the optimum setting. The outcome listed in Tab. 3 shows that the method is also very robust under parameter variations.

Yosemite with clouds			
σ	α	γ	AAE
0.8	80	100	1.94°
0.4	80	100	2.10°
1.6	80	100	2.04°
0.8	40	100	2.67°
0.8	160	100	2.21°
0.8	80	50	2.07°
0.8	80	200	2.03°

Table 3. Parameter variation for our method with spatio-temporal smoothness assumption.

3D - spatio-temporal method					
reduction factor η	outer fixed point iter.	inner fixed point iter.	SOR iter.	computation time/frame	AAE
0.95	77	5	10	23.4s	1.94°
0.90	38	2	10	5.1s	2.09°
0.80	18	2	10	2.7s	2.56°
0.75	14	1	10	1.2s	3.44°

Table 4. Computation times and convergence for Yosemite sequence with clouds.

Although our paper does not focus on fast computation but on high accuracy, the implicit minimisation scheme presented here is also reasonably fast, especially if the reduction factor η is lowered or if the iterations are stopped before full convergence. The convergence behaviour and computation times can be found in Tab. 4. Computations have been performed on a 3.06 GHz Intel Pentium 4 processor executing C/C++ code.

For evaluating the performance of our method for real-world image data, the *Ettlinger Tor* traffic sequence by Nagel was used. This sequence consists of 50 frames of size 512×512. It is available at `http://i21www.ira.uka.de/image_sequences/`. In Fig. 2 the computed flow field and its magnitude are shown. Our estimation gives very realistic results, and the algorithm hardly suffers from interlacing artifacts that are present in all frames. Moreover, the flow boundaries are rather sharp and can be used directly for segmentation purposes by applying a simple thresholding step.

6 Conclusion

In this paper we have investigated a continuous, rotationally invariant energy functional for optical flow computations based on two terms: a robust data term with a brightness constancy and a gradient constancy assumption, combined with a discontinuity-preserving spatio-temporal TV regulariser. While each of these concepts has proved its use before (see e.g. [22, 26]), we have shown that their combination outperforms all methods from the literature so far. One of the main reasons for this performance is the use of an energy functional with *non-linearised* data term and our strategy to consequently postpone all linearisations to the *numerical* scheme: *While linearisations in the model immediately compromise the overall performance of the system, linearisa-*

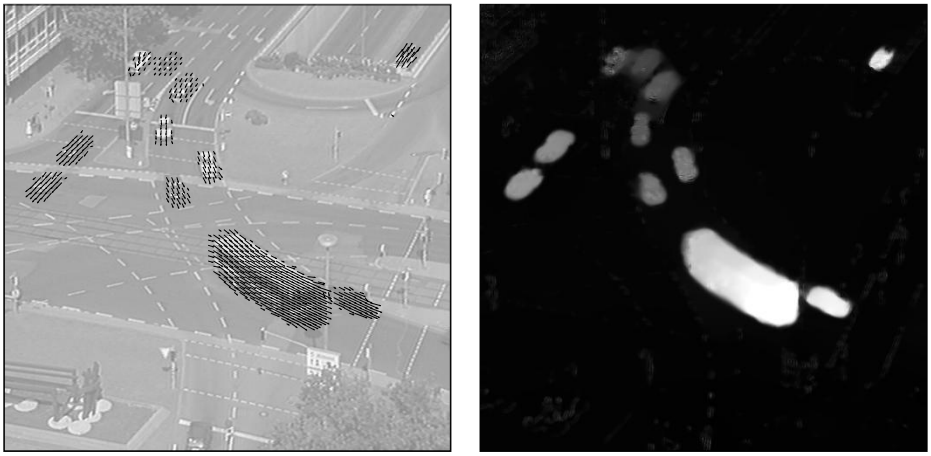

Fig. 2. *(a) Left:* Computed flow field between frame 5 and 6 of the *Ettlinger Tor* traffic sequence. *(b) Right:* Computed magnitude of the optical flow field.

tions in the numerical scheme can help to improve convergence to the global minimum. Another important result in our paper is the proof that *the widely-used warping can be theoretically justified as a numerical approximation strategy that does not influence the continuous model*. We hope that this strategy of transparent continuous modelling in conjunction with consistent numerical approximations shows that excellent performance and deeper theoretical understanding are not contradictive: They are nothing else but two sides of the same medal.

References

1. L. Alvarez, J. Esclarín, M. Lefébure, and J. Sánchez. A PDE model for computing the optical flow. In *Proc. XVI Congreso de Ecuaciones Diferenciales y Aplicaciones*, pages 1349–1356, Las Palmas de Gran Canaria, Spain, Sept. 1999.
2. L. Alvarez, J. Weickert, and J. Sánchez. Reliable estimation of dense optical flow fields with large displacements. *International Journal of Computer Vision*, 39(1):41–56, Aug. 2000.
3. P. Anandan. A computational framework and an algorithm for the measurement of visual motion. *International Journal of Computer Vision*, 2:283–310, 1989.
4. A. Bab-Hadiashar and D. Suter. Robust optic flow computation. *International Journal of Computer Vision*, 29(1):59–77, Aug. 1998.
5. J. L. Barron, D. J. Fleet, and S. S. Beauchemin. Performance of optical flow techniques. *International Journal of Computer Vision*, 12(1):43–77, Feb. 1994.
6. M. J. Black and P. Anandan. Robust dynamic motion estimation over time. In *Proc. 1991 IEEE Computer Society Conference on Computer Vision and Pattern Recognition*, pages 292–302, Maui, HI, June 1991. IEEE Computer Society Press.
7. M. J. Black and P. Anandan. The robust estimation of multiple motions: parametric and piecewise smooth flow fields. *Computer Vision and Image Understanding*, 63(1):75–104, Jan. 1996.
8. I. Cohen. Nonlinear variational method for optical flow computation. In *Proc. Eighth Scandinavian Conference on Image Analysis*, volume 1, pages 523–530, Tromsø, Norway, May 1993.

9. R. Deriche, P. Kornprobst, and G. Aubert. Optical-flow estimation while preserving its discontinuities: a variational approach. In *Proc. Second Asian Conference on Computer Vision*, volume 2, pages 290–295, Singapore, Dec. 1995.
10. G. Farnebäck. Very high accuracy velocity estimation using orientation tensors, parametric motion, and simultaneous segmentation of the motion field. In *Proc. Eighth International Conference on Computer Vision*, volume 1, pages 171–177, Vancouver, Canada, July 2001. IEEE Computer Society Press.
11. B. Horn and B. Schunck. Determining optical flow. *Artificial Intelligence*, 17:185–203, 1981.
12. S. Ju, M. Black, and A. Jepson. Skin and bones: multi-layer, locally affine, optical flow and regularization with transparency. In *Proc. 1996 IEEE Computer Society Conference on Computer Vision and Pattern Recognition*, pages 307–314, San Francisco, CA, June 1996. IEEE Computer Society Press.
13. S.-H. Lai and B. C. Vemuri. Reliable and efficient computation of optical flow. *International Journal of Computer Vision*, 29(2):87–105, Oct. 1998.
14. M. Lefébure and L. D. Cohen. Image registration, optical flow and local rigidity. *Journal of Mathematical Imaging and Vision*, 14(2):131–147, Mar. 2001.
15. B. Lucas and T. Kanade. An iterative image registration technique with an application to stereo vision. In *Proc. Seventh International Joint Conference on Artificial Intelligence*, pages 674–679, Vancouver, Canada, Aug. 1981.
16. E. Mémin and P. Pérez. A multigrid approach for hierarchical motion estimation. In *Proc. Sixth International Conference on Computer Vision*, pages 933–938, Bombay, India, Jan. 1998. Narosa Publishing House.
17. E. Mémin and P. Pérez. Hierarchical estimation and segmentation of dense motion fields. *International Journal of Computer Vision*, 46(2):129–155, 2002.
18. H.-H. Nagel. Extending the 'oriented smoothness constraint' into the temporal domain and the estimation of derivatives of optical flow. In O. Faugeras, editor, *Computer Vision – ECCV '90*, volume 427 of *Lecture Notes in Computer Science*, pages 139–148. Springer, Berlin, 1990.
19. H.-H. Nagel and W. Enkelmann. An investigation of smoothness constraints for the estimation of displacement vector fields from image sequences. *IEEE Transactions on Pattern Analysis and Machine Intelligence*, 8:565–593, 1986.
20. L. I. Rudin, S. Osher, and E. Fatemi. Nonlinear total variation based noise removal algorithms. *Physica D*, 60:259–268, 1992.
21. C. Schnörr. Segmentation of visual motion by minimizing convex non-quadratic functionals. In *Proc. Twelfth International Conference on Pattern Recognition*, volume A, pages 661–663, Jerusalem, Israel, Oct. 1994. IEEE Computer Society Press.
22. M. Tistarelli. Multiple constraints for optical flow. In J.-O. Eklundh, editor, *Computer Vision – ECCV '94*, volume 800 of *Lecture Notes in Computer Science*, pages 61–70. Springer, Berlin, 1994.
23. S. Uras, F. Girosi, A. Verri, and V. Torre. A computational approach to motion perception. *Biological Cybernetics*, 60:79–87, 1988.
24. J. Weickert, A. Bruhn, and C. Schnörr. Lucas/Kanade meets Horn/Schunck: Combining local and global optic flow methods. Technical Report 82, Dept. of Mathematics, Saarland University, Saarbrücken, Germany, Apr. 2003.
25. J. Weickert and C. Schnörr. A theoretical framework for convex regularizers in PDE-based computation of image motion. *International Journal of Computer Vision*, 45(3):245–264, Dec. 2001.
26. J. Weickert and C. Schnörr. Variational optic flow computation with a spatio-temporal smoothness constraint. *Journal of Mathematical Imaging and Vision*, 14(3):245–255, May 2001.